Journal of Molecular Structure 1171 (2018) 834–842

Contents lists available at ScienceDirect

Journal of Molecular Structure

journal homepage: http://www.elsevier.com/locate/molstruc

Synthesis, characterization, DFT studies of piperazine derivatives and its Ni(II), Cu(II) complexes as antimicrobial agents and glutathione reductase inhibitors

Neslihan Özbek [a, *], Serhat Mamaş [b], Türkan Erdoğdu [b], Saliha Alyar [c], Kerem Kaya [d], Nurcan Karacan [b]

[a] Department of Primary Education, Faculty of Education, Ahi Evran University, Kırşehir, Turkey
[b] Department of Chemistry, Science Faculty, Gazi University, Ankara, Turkey
[c] Department of Chemistry, Science Faculty, Karatekin University, Çankırı, Turkey
[d] Department of Chemistry, Faculty of Science and Letters, Istanbul Technical University, Istanbul, Turkey

ARTICLE INFO

Article history:
Received 11 May 2018
Received in revised form
16 June 2018
Accepted 18 June 2018
Available online 19 June 2018

Keywords:
Piperazine
Cyclic voltammetry
Glutathione reductase
HOMO-LUMO
MIC

ABSTRACT

1,4-Piperazinediacetic acid and 1,4-diethyl ester (**1**) were prepared by treating 1,4-piperazine with ethylchloroacetate; and its structure was identified by single crystal X-ray diffraction analysis. Then, 1,4-piperazinediacetic acid, 1,4-dihydrazide (**2**) and its metal complexes (**2-Ni(II)** and **2-Cu(II)**) were synthesized, respectively. Their structures were characterized by elemental analysis, ESI-MS, IR and NMR spectral data. The electrochemical behavior of compounds was investigated using cyclic voltammetry (CV). The density functional theory (DFT) was used for geometry optimization, HOMO and LUMO energies, HOMO–LUMO energy gap and dipole moment of the compounds. It has been observed that the calculated band gaps for complexes are much smaller than ligands. Furthermore, ^{13}C and ^{1}H NMR analyses of **(1)** and **(2)** compounds were performed at B3LYP/6-311++G(d,p) level of theory and compared with the experimental findings. Observed ^{13}C and ^{1}H NMR chemical shifts were very good agreement with calculated chemical shifts. The antibacterial activities of synthesized compounds were studied against three Gram-positive and three Gram-negative bacteria by using the microdilution and disk diffusion methods. Baker's yeast glutathione reductase and human erythrocyte glutathione reductase were evaluated for all compounds. Copper (II) complex has the most inhibition activities against glutathione reductase enzyme in all compounds.

1. Introduction

Hydrazides attrack the attention of medicinal chemists because they enable the synthesis of different compounds [1], therefore, they possess different pharmaceutical activities such as antibacterial [2], antifungal [3], anticancer [4], anti-inflammatory [5], antituberculosis [6].

Piperidine scaffolds are found in various natural products and bio-active molecules of many synthetic pharmaceuticals [7–11]. Piperidine derivatives exhibit several biological properties including antitumor [12], antidepressant [13], antibacterial [14] and antifungal etc [15]. Zikova et al. reported that symmetric piperazine esters having various biological activity such as central nervous system, autonomic nervous system, cardiovascular system were less toxic than their asymmetric analogues [16].

A literature survey revealed that, piperazines and hydrazides, possessing flexible binding feature, exhibit various inhibitory potencies against acetylcholinesterase [7,17], diaminopimelate aminotransferase [18], diacylglycerol acyltransferase [19], monoamine oxidase [20], focal adhesion kinase [10], glycogen synthase kinase [21]. However, research on glutathione reductase activities of this kind of compounds is relatively few [22–24]. Furthermore, it is known that ligands, schiff bases and their metal complexes utilized as starting materials in the synthesis of organic or inorganic compounds for industrial usage.

The biological activities of 1,4-piperazinediacetic acid, 1,4-dihydrazide **(2)** and its parent compound, 1,4-piperazinediacetic acid, 1,4-diethyl ester **(1)** were not well investigated except for

* Corresponding author.
E-mail address: ege_nesliozbek@hotmail.com (N. Özbek).

https://doi.org/10.1016/j.molstruc.2018.06.076
0022-2860/

anti tubercular activity of **(2)** [25]. In this paper, **[2-Ni(II)]** and **[2-Cu(II)]** complexes of **(2)** derived from **(1)** were synthesized and characterized by using elemental analyses, FT-IR, LC-MS, spectrometric methods, magnetic susceptibility and conductivity measurements methods for the compounds. (1) has also been characterized by single crystal X-ray diffraction. ^{1}H and ^{13}C shielding tensors for **(1)** and **(2)** were calculated with GIAO/DFT/B3LYP/6-311G++(d, p) basis set in DMSO phase. The antibacterial activies of synthesized compounds were studied against Gram positive bacteria: *Salmonella typhimurium* ATCC 14028, *Staphylococcus aureus* ATCC 25923 *Enterococcus faecalis* ATCC 29212, Gram negative bacteria: *Escherichia coli* ATCC 25922, *Klebsiella pneumonia* ATCC 27853, *Pseudomonas aeruginosa* ATCC 27853 by using microdilution method (as MICs) and disk diffusion method. The inhibition activities of these compounds on baker's yeast glutathione reductase and human erythrocyte glutathione reductase evaluated. The electrochemical behaviors of piperazine derivatives were investigated by cyclic voltammetry (CV), controlled potential electrolysis and chronoamperometry (CA) techniques.

2. Experimental

2.1. Materials

Piperazine, hydrazine hydrate, ethyl chloroacetate, potassium carbonate, nickel (II) chloride hexahydrate, copper (II) chloride dihydrate (all from Sigma-Aldrich) and solvents (all from Merck) were used without further purification. All chemicals and solvents used in synthesis were of analytical grade.

2.2. Physical measurements

The elemental analyses (C, H, N and S) were performed on a LECO CHNS 9320 type elemental analyzer. ^{1}H -NMR and ^{13}C -NMR spectra were recorded on a Bruker- Spectrospin Avance DPX-400 Ultra-Shıeld. TMS was used as internal standard and deuteriated DMSO as solvent. The IR spectra (4000-400 cm^{-1}) were recorded on a Mattson 1000 FT-IR Spectrophotometer with samples prepared as KBr pellets. LC/MS-APCI was recorded on an Waters 2695 Alliance Micromass ZQ Spectrometer. The melting points were measured using an Opti Melt apparatus. TLC was conducted on 0.25 mm silica gel plates (60F254, Merck). The molar magnetic susceptibilities were measured on powdered samples using Gouy method. The molar conductance measurements were carried out using a Siemens WPA CM 35 conductometer. Thermogravimetric analysis (TG/DTG curves) was carried out by Du Pont Instrument 951 TGA ± DTA apparatus.

2.3. Synthesis of 1,4-piperazinediacetic acid, 1,4-diethyl ester (1)

An ethanol solution of piperazine (2,13 g, 0,02 mol) was added drop wise to ethanol solution of ethyl chloroacetate (6,01 g, 0,04 mol) and potassium carbonate (2,76 g, 0,02 mol) maintaining the temperature at about 323 K. Then, the mixture was stirred for 24 h at room temperature. After the completion of the reaction, solvent was distilled off and the residue was poured into ice water. The precipitated solid was filtered off, dried and recrystallized from appropriate solvents. The synthesized compound was purified with suitable solvents. Purity of compound was checked by TLC [26]. Yield 75%. M.p. 177–179 °C. Elemental analysis for $C_{12}H_{22}N_2O_4$ (MW: 258.32 g/mol) (Calc.%) C, 55.80; H, 8.58; N,10.84; O, 24.77. (Found %) C, 54.89; H, 7.98; N, 11.42; O, 25.17. IR(KBr) cm^{-1}: 2917 cm^{-1} (CH)aliph, 1229 cm^{-1} (CN), 1619 cm^{-1} (C=O). LC-MS: m/z (abudance %) $[M+1]^+$: 259.81(100%)

2.4. Synthesis of 1,4-piperazinediacetic acid, 1,4-dihydrazide (2)

1,4-Piperazinediacetic acid, 1,4-diethyl ester (1,4 g, 0,005mol) in ethanol (30 mL) was added drop wise to solution of hydrazine hydrate (3.0 mL) in ethanol while the temperature was maintained between 268 and 273 K. The mixture was stirred for 24 h mean while the completion of the reaction was monitored by TLC and then, the solvent was evaporated. The colorless crude compound was purified in ethanol/water (3:1) by column chromatography and then the product was recrystallized from ethanol/water mixture (3:1) [27]. Yield 87%. M.p. 195–197 °C. Elemental analysis for $C_8H_{18}N_6O_2$ (MW:230.27 g/mol) (Calc.%) C, 41.73; H, 7.88; N, 36.50; O, 13.90. (Found %) C, 42.01; H, 8.11; N, 35.45; O, 13.33. IR(KBr) cm^{-1}: 2927 cm^{-1} (CH)aliph, 3286 cm^{-1} (NH_2), 3164 cm^{-1} (NH), 1660 cm^{-1} (C=O). LC-MS: m/z (abudance %) $[M+1]^+$: 231,2 (100%).

2.5. Synthesis of Ni(II) and Cu(II) complexes [2-Ni(II), 2-Cu(II)]

All metal complexes were prepared by the following general method: To solution of **(2)** (2.0 mmol) in methanol/water (3:1) (2.0 mL), metal chlorides (2,0 mmol) in methanol (20 mL) was added drop wise by heating on magnetic stirrer. The metal complexes were precipitated at room temperature and filtered off, dried in a desiccator over $CaCl_2$ [28–30].

[2-Ni(II)]: Yield 67%. M.p.>280 °C. C_8H_{16} $N_6O_2NiCl_2$ (MW: 356.01 g/mol). IR(KBr) cm^{-1}: 2929 cm^{-1} (CH)aliph, 3187 cm^{-1} (NH_2), 3170 cm^{-1} (NH), 1642 cm^{-1} (C=O), 535 cm^{-1} (Ni–O), 420 cm^{-1} (Ni–N). LC-MS: m/z (abudance %) $[L + Ni + Cl]^+$: 323.5 (18.9%), $[L + Ni]+$: 287.4 (22%), $[L+1]+$: 231,2(100%). $\Lambda_m = 4.0\ \Omega^{-1}\ cm^2.mol^{-1}$ (DMF)

[2-Cu(II)]: Yield 71%. M.p.>300 °C. C_8H_{16} $N_6O_2CuCl_2$ (MW: 361.0 g/mol). IR(KBr) cm^{-1}: 2925 cm^{-1} (CH)aliph, 3192 cm^{-1} (NH_2), 3168 cm^{-1} (NH), 1622 cm^{-1} (C=O), 554 cm^{-1} (Cu–O), 432 cm^{-1} (Cu–N). LC-MS: m/z (abudance %) $[L + Cu]^+$: 293,3 (11%), $[L + Cu+2Cl]^+$: 366.2 (17%). $\Lambda_m = 7.0\ \Omega^{-1}\ cm^2.mol^{-1}$ (DMF)

2.6. Single crystal X-Ray crystallography

The single crystal of **(1)** with dimensions 0.01 × 0.20 × 0.40 mm was grown by slow evaporation of ethylacetate solution. It was mounted on a micromount, attached to a goniometer head on a Bruker D8 VENTURE diffractometer equipped with PHOTON100 detector and measured with graphite monochromated Mo-Kα radiation (λ = 0.71073 Å) using 1.0° of only Ω rotation frames at room temperature, respectively. The structure has been solved by intrinsic method SHELXS-19 [31] and refined SHELXL-2014/7 [32]. Molecular drawings are generated using OLEX2. Ver. 1.2-dev [33]. Thermal ellipsoids are plotted in Fig. 1 and the crystal packing structure of (**1**) is also exhibited in Fig. 1S. Crystal data and structure refinement parameters are given in Table 1S. The selected bond lengths and bond angles of single crystal are listed in Table 2S. CCDC 1820087 contains the supplementary crystallographic data for **(1)**. Further details on crystal data, data collection, and refinements can be found on the supporting information.

2.7. Electrochemical studies

Voltametric measurements were carried out with CHI 760 d Electrochemical Analyzer. Glassy carbon electrode (BAS MF-2012), bulk electrolysis electrode (BAS MF-1056) and 11 μm-ultramicro carbon electrodes (BAS MF-2007) were used as a working electrode. The electrodes were polished with 1 μm, 0.3 μm and 0.05 μm alümina slurries made from dry Buehler alumina and ultra-pure water (16 MΩcm) on polishing microcloth before each use. A platinum wire was used as the auxiliary electrode (BAS MW-

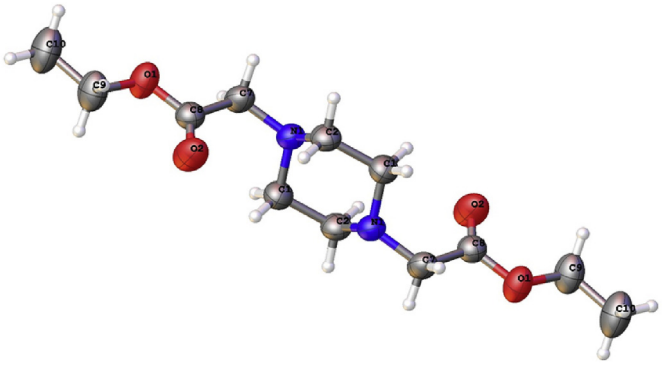

Fig. 1. ORTEP drawing of 1 with atom labeling scheme. Ellipsoids are drawn at 50% probability level.

1032). The reference electrode was a silver wire in contact with 0.01 M $AgNO_3$ in dimethylsulfoxide (BAS MF-2052). All solutions were deairated for 15 min with pure nitrogen gas. All measurements were taken at room temperature, 20 ± 1 °C. In voltammetric measurements, the background currents were automatically subtracted from originally obtained currents.

The number of electrons transferred and diffusion coefficients were determined by ultramicro electrode CV technique of Baranski [34] and also, the heterogeneous rate constants were calculated according to Klingler-Kochi method [35]. Also, the data obtained from bulk electrolysis were used to calculate the number of electrons transferred (n).

2.8. Glutathione reductase activity assay

Activity of glutathione reductase (GR) was determined according to the standard protocol [36]. Glutathione reductase activity was expressed as μmole NADPH oxidized per minute per mg protein, at pH 6.9 at 25 °C, using a molar extinction coefficient at 340 nm of 6.2 mM $^{-1}cm^{-1}$ for NADPH. Decrease in the absorbance at 340 nm due to oxidation of NADPH was monitored. The standard GR reaction medium contains 20.5 mM KH_2PO_4, 26.5 mM K_2HPO_4, 200 mM KCl, 1 mM EDTA, (pH 6.9), yeast GR (1.0 units/mL), NADPH (0.2 mM), GSSG (1 mM). The final volume of the assay mixture was left at 1.0 mL. The reaction mixture was carefully mixed and after 3 min pre-incubation at 25 °C, the reaction was started by the addition of NADPH, and time-dependent changes in absorbance at 340 nm were monitored. GR activity was measured for 1 min in the quartz cuvette. The reaction was continuing linearly during this time period. The initial velocity of GR reaction was measured by the slope of recorded tracing. Ten measurements were performed and mean values were used for each data point. GR activity of control measured without addition of compounds was equal to about 18 μmole NADPH per min per mg protein. The enzyme activities in the absence of the inhibitors were taken as 100%. 1 mM stock solutions of the compounds were prepared by dissolving in minimum amount of dimethyl sulfoxide (DMSO) and diluting with water. Activity values and inhibitor concentrations were graphed. Inhibitor concentrations at the half of activity were determined as IC_{50} values [37].

2.9. Theoretical calculations

Because of the effective bioactivities of piperazine compounds, the three dimensional conformation analysis was performed to obtain important previews about molecular behavior in gas and solution forms. To determine the most stable structure, all the possible conformations of apmsh were obtained by potential energy scan. One-dimensional potential energy scans were performed for four torsion angles-τ1 C10–C9–O1–C8, τ2 O1–C8–C7–N1, τ3 C9–O1–C8–O2 and τ4 O2–C8–C7–N1 in the full range of $0–360^0$, DFT method. In the mentioned conformational analysis, the molecular geometry optimizations was compared with the Gaussian 03 W software package by using DFT approaches in addition to the determination of crystal structure (Fig. 2) [38]. The split valence 6-311++G (d, p) basis set was used for the expansion of the molecular orbital [39]. The geometries were fully optimized without any constraint with the help of an analytical gradient procedure implemented within the Gaussian 03 W program. The ^1H and ^{13}C NMR chemical shifts of the compounds were calculated in $CDCl_3$ using the GIAO method. The energy gap of HOMO-LUMO explains the prospective charge transfer interaction within the molecule, and in this study, the frontier orbital energy gap was obtained at B3LYP method using 6-311++G(d,p) basis set.

2.10. Procedure for antibacterial activity

Salmonella typhimurium ATCC 14028, *Staphylococcus aureus* ATCC 25923 *Enterococcus faecalis* ATCC 29212, *Escherichia coli* ATCC 25922, *Klebsiella pneumonia* ATCC 27853, *Pseudomonas aeruginosa* ATCC 27853 cultures were obtained from Gazi University, Biology Department and bacterial strains were cultured overnight at 310 K in a nutrient broth. During the survey, these stock cultures were stored in the dark at 277 K. The inocula of microorganisms were prepared from broth cultures and suspensions were adjusted to 0,5 McFarland standart turbidity.

The piperazine derivatives and their complexes were dissolved in dimethylsulfoxide (10%DMSO) to a final concentration of 8.0 mg mL^{-1} and sterilized by filtration with 0,45 μm millipore filters. Antimicrobial tests were then carried out by the disc diffusion method using 100 μL of suspension containing 10^8 CFU mL^{-1} bacteria which was spread on nutrient agar (NA) medium. The discs (6 mm in diameter) impregnated with 30 μL of each compound (240 μg/disc) at the concentration of 8.0 mg mL^{-1} and placed on the inoculated agar. DMSO impregnated discs were used as negative control. Sulfisoxazole (300 μg/disc) were used as positive control to determine the sensitivity of one strain/isolate in each microbial species tested. The inoculated plates were incubated at 37 °C for 24 h for bacterial strains isolates. Antimicrobial activity in the disc diffusion assay was evaluated by measuring the zone of inhibition against the test organisms. Each assay in this experiment was repeated twice [40] Percentage of inhibition was calculated by comparing the distance of the sample to the distance of Sulfisoxazole as standard [41].

The minimum inhibitory concentration (MIC) values of the piperazine derivatives and their complexes were determined using modification of the micro well dilution assay method. 100 μL of the test compounds, initially prepared at 4000 μg mL^{-1} concentration, were added into the first wells. Then, 100 μL of the serial dilutions was transferred into nine consecutive wells. The contents of the wells were mixed and the micro plates were incubated at 37 °C for 24 h. The compounds were tested against each microorganism twice. The values obtained are average of the two results. The MIC values were determined from visual examinations as the lowest concentration of the extracts in the wells with no bacterial growth [42].

3. Results and discussion

3.1. Characterization of the complexes

The reaction mechanisms are exhibited in Fig. 3. All complexes

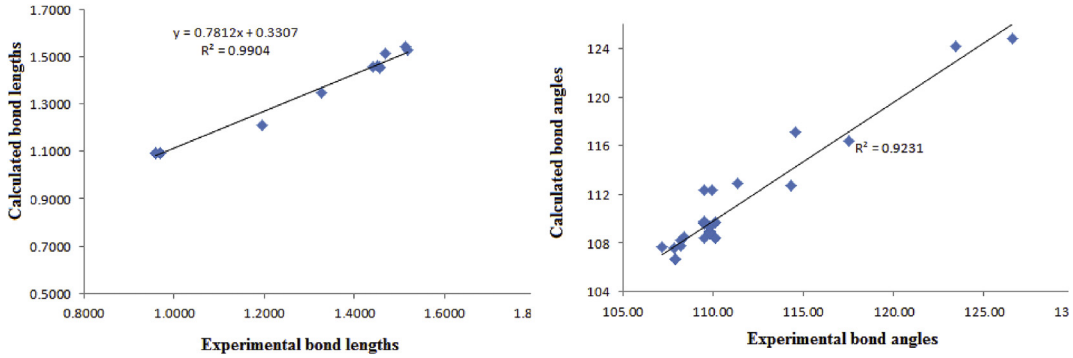

Fig. 2. Correlation values of (2).

are stable under normal conditions. Upon heating, decomposition occurs. Complexes are soluble in both DMSO and DMF, but insoluble in both ethanol and acetonitrile. The elemental analysis results show that **[2-Ni(II)]** and **[2-Cu(II)]** complexes have 1:1 (metal:-ligand) stoichiometry. The analytical results are in good agreement with those required mole ratio by the general formula $[MLCl_2].H_2O$. In order to inspect the binding of Schiff base ligand to the metal ions, the FT-IR spectrum of the free ligand was compared with that of the transition metal complexes. The bands of **(2)** at 1660 cm^{-1} and 3286 cm^{-1} were attributed to the stretching vibration of the υ(C═O) and υ(NH_2), respectively. The complexes reveals that υ(C═O) in the range of 1642–1622 cm^{-1} and υ(NH_2) in the range of 3187–3190 cm^{-1}, respectively. The decrease in frequencies of the C═O and NH_2 bonds are indicative of the ligand chelation through amine-N and carbonyl-O into the metal center as a result of the withdrawal of electron density from the nitrogen and oxygen atoms. The υ(M-O) and υ(M-N) vibrations are observed at lower frequencies as expected. The low-frequency skeletal vibrations due to υ(M-O) and υ(M-N) stretching provided direct evidence for the complexation [43]. Orojloo et al. have reported bands in the region of 540–490 cm^{-1} for υ(M-O) and 450–400 cm^{-1} for υ(M-N) vibrations, respectively [44]. In present study, υ(M-O) vibration occurring in the region 535-554 cm^{-1} and υ(M-N) vibration occurring in the region 420-432 cm^{-1} has been assigned for metal complexes.

Conductivity measurements in non-aqueous solutions have been frequently used in structural studies of metal chelates within the limits of their solubilities. They provide a method for testing degree of ionization of the complexes. The number of molar ions in the solution can be determined by molar conductivity measurements. The non-ionized complexes have negligible value of molar conductance. The molar conductivities of the solid chelates are measured in 10^{-3} mol solution of 1:1 complexes in DMSO. The product of the cell constant and the measured conductance of the solution give the specific conductivity, K. The molar conductivity (Ω^{-1} cm^2 mol^{-1}) is given by the relation: $\Lambda m = K/C \times 1000$ where C (mol/L) is the concentration of the solution. It is clear from the conductivity data that our metal complexes behave as weak electrolytes. The molar conductance values indicate that the anions may be presented inside the coordination sphere or absent. This result was confirmed from the chemical analysis where Cl ions are not precipitated by the addition of $AgNO_3$ solution. All the complexes did not show electrolytic properties [45].

The electronic spectra of (**2-Ni(II)**) complex shows three absorption band in the region 10,005–10,123 cm^{-1}, 16,388-17330 cm^{-1} and 24,891–24,999 cm^{-1}, which were assigned to $^3A_{2g}/^3T_{2g}$ (υ 1), $^3A_{2g}/^3T_{1g}$ (υ 2) and $^3A_{2g}/^3T_{1g}$ transitions, respectively. These are the characteristic bands of octahedral environment around Ni(II) ion. Magnetic moment value of Ni(II) complex (2.9 B M.) confirms the presence of two unpaired electrons in the octahedral geometry [46]. · The electronic spectra of(**2-Cu(II)**) complex shows a maximum broad band at 16,393 cm^{-1}. This band is assigned to $^2E_g/^2T_{2g}$ transition in the octahedral Cu(II) complex [47]. The magnetic moment of Cu(II) complex is in agreement with the value of the octahedral geometry (1.8 B M) [48].

In order to identify the thermal stability of the metal complexes,

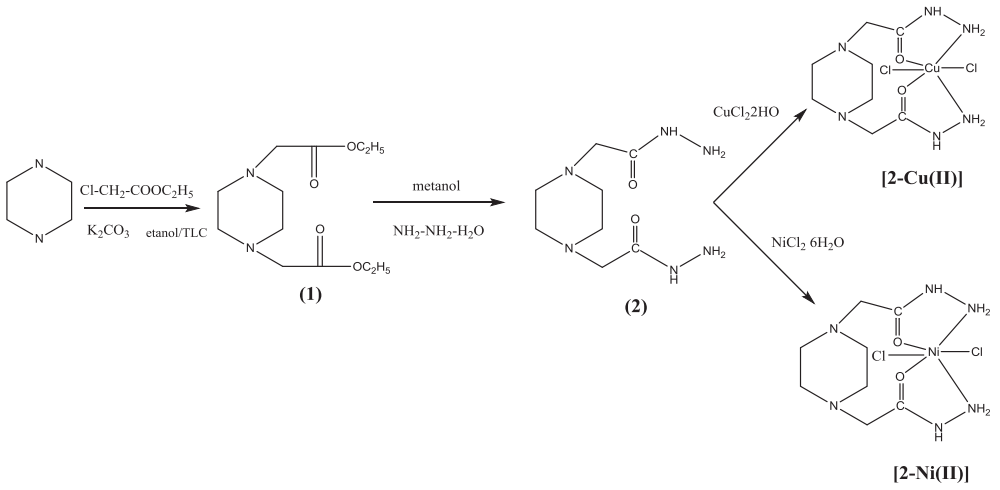

Fig. 3. Preparation of compounds.

the thermal decomposition studies were carried out using thermogravimetry techniques with in the temperature range from 25 °C to 1200 °C under an N_2 atmosphere. The water analysis of the complexes suggested one water molecule in the structure of metal complexes. Thermal analysis of Ni (II) complex indicates loss of weight in the following two steps: a small weight loss in the range of 50–150 °C due to loss of lattice water in the first step, maximum weight loss above 250 °C in the second step which can be assigned to complete decomposition of the ligand moity around the metal ion. As seen in Fig. 2S, there are mainly three continuous mass loss steps in the TGA curve of Cu(II) complex. The first step with mass loss of 5.2% from 0 to 155 °C may be assigned to the loss of lattice water. There is mainly large mass loss step after 220 °C with loss percentage of 59.7% which is attributed to the organic decomposition.

3.2. X-ray crystallography

Compound **(1)** was crystallized in a monoclinic lattice with P1 21/c1 space group. The unit cell contains 2 molecules and the crystal lattice does not contain any intramolecular or intermolecular interactions. The asymmetric unit of the title compound contains only one half-molecule of the structure **(1)**. The six-membered piperazine ring adopts a standard chair conformation. Torsion angles of C1–N1–C2–C1 and N1–C1–C2–N1 observed as 58.7° and 57.6° (Table 2S) also proves the chair conformation [49]. The two carboxylate groups are mutually in *trans* isomery. The C–N single bond distance of the ring (1.458(2) Å) is in agreement with other crystals of piperazine [50,51].

3.3. Electrochemical behavior

The electrochemical behavior of compounds in DMSO at glassy carbon electrode were investigated using cyclic voltammetry (CV), controlled potential electrolysis and chronoamperometry (CA) techniques. Reduction peak potentials (E_p^c) of compounds at different scaning rates are presented in Figs. 4–5This CV has demonstrated that investigated compounds has two-tree reduction peaks at glassy carbon electrode in DMSO. It is also observed in Figs. 4–5 that the peak potentials show a negative shift by increasing of the scan rate. The fact that, E_p^c values show a negative shift at higher scan rates is a clear indication of an irreversible behavior.

3.4. Determination of the number of electrons transferred and the diffusion coefficient

The number of electrons transferred (n) during the reduction process and the diffusion coefficient (D) of the compounds were determined by using ultramicro electrode and chronoamperometry methods, n and D values were calculated as follows:

$$n = \frac{n_s S^2 i_s C_s}{S_s^2 i C} \qquad D = \frac{D_s \; S_s^2 \; i^2}{S^2 \; i_s^2}$$

where is limiting steady-state current, S is the slope of the of the chronoamperometric i vs $t^{-1/2}$ plot.

Klingler-Kochi Method for Determination of the Heterogeneous Electron-Transfer Standard Rate Constants.

The limiting steady-state current of compound was determined by linear sweep voltammetry method. The diffusion coefficient (D) is related with the diffused amount of compound to the electrode surface [52,53]. The heterogeneous standard rate constant (k_s) is found by cyclic voltammogram at different scan rates. In general, increasing the scan rate affects the reduction peak potential (E_p^c) and the peak width values ($E_{p/2}$) which change the value of k_s calculated from the formula given below. The heterogeneous standard rate constant (k_s) at 21 °C which are independent of Table 1 and they are the indicator of irreversible behavior [34,35].

$$K_s = 2.18\left(\frac{D\beta nF\nu}{RT}\right)^{1/2} \qquad \beta = 1.857\frac{RT}{nF\left(E_p^c - E_{p/2}^c\right)}$$

The current function decreasing exponentially towards the higher scan rates is an indication of the electron transfer followed by electrochemical reduction (EC) mechanism. It is supposed that $2e^-$ transferred reductions occur. The action mechanism of compounds can be useful for pharmacokinetic and pharmacodynamic purposes in biological systems as drugs.

This work has demonstrated that our compounds have two-tree reduction peaks at glassy carbone electrode in DMSO. The electrochemical reduction occurs through two electrons by successive two electron irreversible peaks followed by chemical reactions. The number of electrons transferred which was calculated by UME method is in good accordance with the number of electrons determined from bulk electrolysis. Based on the electrochemical results, the reaction mechanism of compounds can be conveniently claimed as EC mechanism. $E_p^c - E_{p/2}^c$ values were found to be 50–130 mV for each peak which is in good agreement with those given in literature for EC systems. The fact that Ep^c values show a

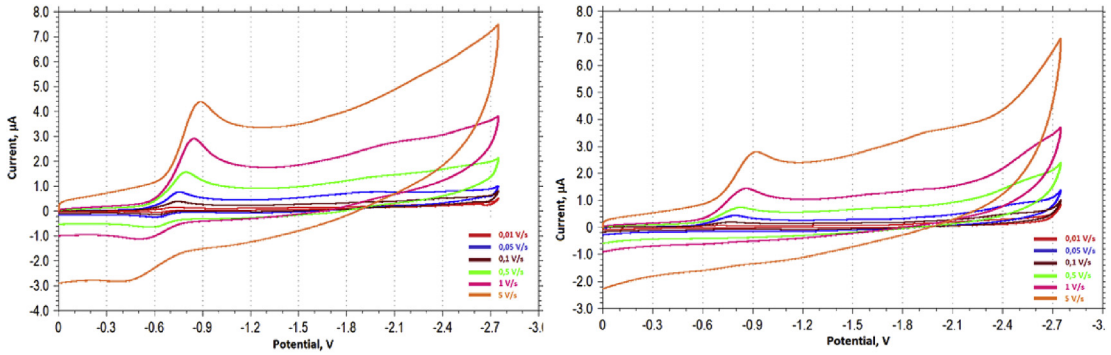

Fig. 4. Cyclic voltamogram (CV) of **(1)** and **(2)** in DMSO containing 0.1 M TBATFB on glassy carbon electrode at a scan rate of 0.01–5 Vs^{-1}(vs. Ag/Ag^+).

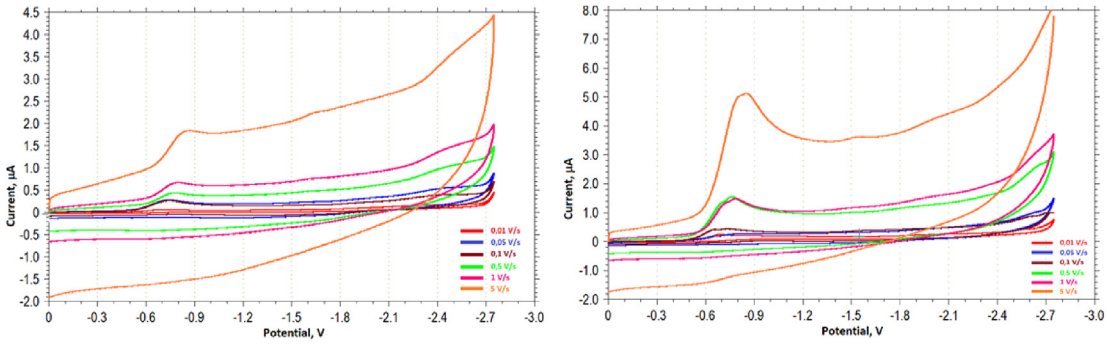

Fig. 5. Cyclic voltamogram (CV) of **[2-Ni(II)]** and **[2-Cu(II)]**in DMSO containing 0.1 M TBATFB on glassy carbon electrode at a scan rate of 0.01–5 Vs^{-1}(vs. Ag/Ag^{+}).

Table 1
Diffusion coefficient, Transferred electron numbers (n), Bulk electrolysis calculated by the number of electrons (n) and heterogeneous rate constant of compounds in DMSO media.

	Cotrell Slope (S)x10^5	Diffusion Coefficient (D, cm^2/s) x 10^7	UME Limit Current, (i_{ss}, A)x10^{10}	n (Baranski Method)	n (Bulk Electrolysis)	Standart Heterogeneous Scan rate *ks(cm/s)x 10^6
(1)	4.85 ± 0.10	2.45 ± 0.08	3.06 ± 0.02	1.96 ± 0.01	1.91 ± 0.02	1.14 ± 0.04
(2)	3.32 ± 0.01	3.06 ± 0.03	3.21 ± 0.05	2.01 ± 0.02	1.99 ± 0.01	2.24 ± 0.03
[2-Ni(II)]	2,15 ± 0.12	5.87 ± 0.01	2.26 ± 0.03	1.94 ± 0.03	1.98 ± 0.02	6.13 ± 0.05
[2-Cu(II)]	1.86 ± 0.08	7.94 ± 0.03	1.92 ± 0.01	2.08 ± 0.01	2.01 ± 0.03	8.28 ± 0.01

Results are average of three measurements and standard deviation.

negative shift at higher scan rates is a clear indication of an irreversible behavior (Figs. 4–5). This was also verified by the decrease of the current function ($i_p^c/v^{1/2}$) with increasing scan rate (v) graphs. This is a further proof that a chemical step takes place after the electron transfer process. It can be supposed that the reactions are not controlled by adsorption phenomenon. The linearity of i_p^c *vs.* $v^{1/2}$ graphs indicates that the reactions are diffusion controlled.

3.5. Glutathione reductases inhibition studies

As seen above, all compounds exhibit the broad-spectrum bactericidal activities. This brings us to further examine their glutathione reductase activities, since the copper(II) complexes of the pyrazine-based hydrazide have been displayed many applications in biological activities. Herein, interaction between the compounds and Baker's yeast glutathione reductase and human erythrocyte glutathione reductases were assayed and evaluated. The results are presented in Table 2.

All compounds were active inhibitor of Baker's yeast and human erythrocyte glutathione reductase. The most active compound in the series was copper(II) complex with IC_{50} value of 63.18 ± 0.28 µM against Baker's yeast glutathione reductase. Ni(II) complex exhibited less activity than copper (II) complex. Pyrazine-based hydrazide **(2)** showed greater inhibitory activity than parent **(1)**.

Table 2
Glutathion reductase inhibitory activities of compounds.

Compounds	IC_{50} (µM)	
	Baker's yeast	Human erythrocyte
(1)	155.28 ± 0.67	186.20 ± 0.59
(2)	108.91 ± 0.46	129.48 ± 0.59
[2-Ni(II)]	78.16 ± 0.55	119.50 ± 0.25
[2-Cu(II)]	63.18 ± 0.28	100.73 ± 0.79

Table 3
Calculated values for frontier orbital energies, energy band gap (ΔE), ionization energy (I), electron affinity(A), electronegativity(χ), chemical hardnesses (η) and chemical softness (S), chemical potential(µ) and electrophilicity index (ω) of studied compounds.

Physical properties	(1)	(2)	[2-Ni(II)]	[2-Cu(II)]
E_{HOMO} (eV)	−7.70	−5.11	−6.24	−5.22
E_{LUMO} (eV)	−0.64	−0.57	−3.66	−3.60
$\Delta E = E_{HOMO\text{-}LUMO}$ (eV)	7.06	4.54	2.58	1.62
I (eV)	7.70	5.11	6.24	5.22
A (eV)	0.64	0.57	3.66	3.60
χ (eV)	4.17	2.84	4.95	4.41
η(eV)	3.53	2.27	1.29	0.81
S (eV^{-1})	0.14	0.22	0.39	0.62
µ(eV)	−4.17	−2.84	−4.95	−4.41
ω(eV)	2.46	1.77	9.50	12.00

3.6. Computational studies

3.6.1. NMR spectra

The NMR spectra (^1H, ^{13}C) of **(1)** and **(2)** were measured and interpreted in DMSO. The ^{13}C NMR and ^1H NMR spectrum of compounds are given in Figs. 3S–4S. The experimental and calculated chemical shift values are shown in Table 3S. In order to facilitate the interpretation of the NMR spectra, quantum-chemical calculations were performed using B3LYP/6-311G++(d, p) basis set in DMSO phase. Isotropic shielding tensors of ^{13}C were changed into chemical shifts by using a linear relationship suggested by Blanco et al. [54] A similar relationship proposed by Silva et al. [55].

In the ^1H NMR spectra of **(1)**; H1, H2, H7, H9 and H10 protons appeared at 3.24 ppm, 3.24 ppm, 4.13 ppm,2.62 ppm and 1.21 ppm were calculated as 3.26 ppm, 3.24 ppm, 4.12 ppm, 2.62 ppm and 1.29 ppm, respectively. In ^{13}C-NMR spectra of **(1);** C1, C2, C7, C8, C9 and C10 carbon signals assigned at 48.06 ppm, 47.54 ppm, 55.86 ppm, 165.47 ppm, 54.74 ppm and 9.48 ppm were calculated as 48.21 ppm, 47.88 ppm, 55.86 ppm, 165.93 ppm, 53.38 ppm and

9.32 ppm, respectively.

In the ^{1}H NMR spectra of **(2)**; H1, H2 and H7 protons appeared at 2.61 ppm, 2.62 ppm and 2.91 ppm were calculated as 2.85 ppm, 2.98 ppm and 2.94 ppm, respectively. A signal were also observed at 8.80 ppm belongs to HN– group (calculated as 8.85 ppm) and at 4.20 ppm belongs to NH_2– group (calculated as 4.52 ppm). In ^{13}C-NMR spectra of **(2);** C1, C2, C7 and C8 carbon signals assigned at 53.14 ppm, 53.14 ppm, 60.34 ppm and 168.65 ppm were calculated as 49.31 ppm, 49.32 ppm, 59.82 ppm and 169.20 ppm, respectively.

3.6.2. Frontier molecular orbital analysis

The HOMO (highest occupied molecular orbital) and the LUMO (lowest unoccupied molecular orbital) orbitals are the main orbitals involved in chemical stability [56]. Molecular orbitals may give an idea of the nature of the reactivity and some structural and physical properties of the molecules. The HOMO represents the ability to accept an electron and LUMO as an electron receiver represents the ability to obtain an electron. The HOMO energy is directly related to the ionization potential, LUMO energy is directly related to the electron affinity. The frontier molecular orbitals (HOMO and LUMO) are mostly the π-antibonding type molecular orbitals in the structure.

The energy difference between HOMO and LUMO orbital (E_{HOMO}-E_{LUMO}) called as energy band gap is a critical parameter in determining molecular electrical transport properties and electronic systems because it is a measure of electron conductivity [57–60]; . The 3D plots of the frontier orbitals in the ground state HOMO and the excited state LUMO are shown in Fig. 6**.** As shown in Fig. 6 and Table 3, the difference between HOMO and LUMO energy levels of the studied compounds are 7.06, 4.54, 2.58 and 1.62 eV for (**1**), (**2**), [**2-Cu(II)**] and [**2-Ni(II)**], respectively.

All the calculated parameters were given in Table 3. According to frontier molecular orbital analyses results, while there is reverse relationship between antibacterial activity, energy band gap (E_{HOMO}-E_{LUMO}) and chemical hardness (η), there is an accurate relationship between antibacterial activity and chemical softness (S) for studied compounds. Antibacterial activity, energy band gap (E_{HOMO}-E_{LUMO}), chemical hardness (η) and chemical softness (S) are in the following orders, respectively;

(1)<(2)<[2-Ni(II)]<[2-Cu(II)]; (1)>(2)>[2-Ni(II)]> [2-Cu(II)]; (1)>(2)>[2-Cu(II)]>[2-Ni(II)]; 1)<(2)<[2-Ni(II)]<[2-Cu(II)]

3.7. Antibacterial activity results

The test compounds were screened in vitro for their antibacterial activity against three Gram-positive species and three Gram-negative species by the disc diffusion and micro dilution methods. The antibacterial activity of the compounds was tested by paper disc diffusion method (Table 4S). The minimum inhibition concentrations (MICs) of the compounds were also determined and compared with reference drug *Sulfisoxazole* (see Table 4). The results were compared with those of the standard drug *Sulfioxazole* (Fig. 5S).

All compounds at low concentration displayed bacteriostatic activity against all bacteria. It is observed that metal complexes of **(2)** have significantly more antimicrobial activities than the corresponding ligand **(2).** This indicates that metal types have profound impact on antibacterial activities. The influence of substituent on pyrazine group is also more significant. This result disclosed that **(2)** with hydrazide moiety was more active than **(1)** ester moiety. Briefly, **[2-Cu(II)]** were found to be the most active against *Pseudomonas aeruginosa ATCC* 27853 with MIC value of 15.125 μg/mL among the all tested compounds and also showed the more potency than *Sulfisoxazole*.

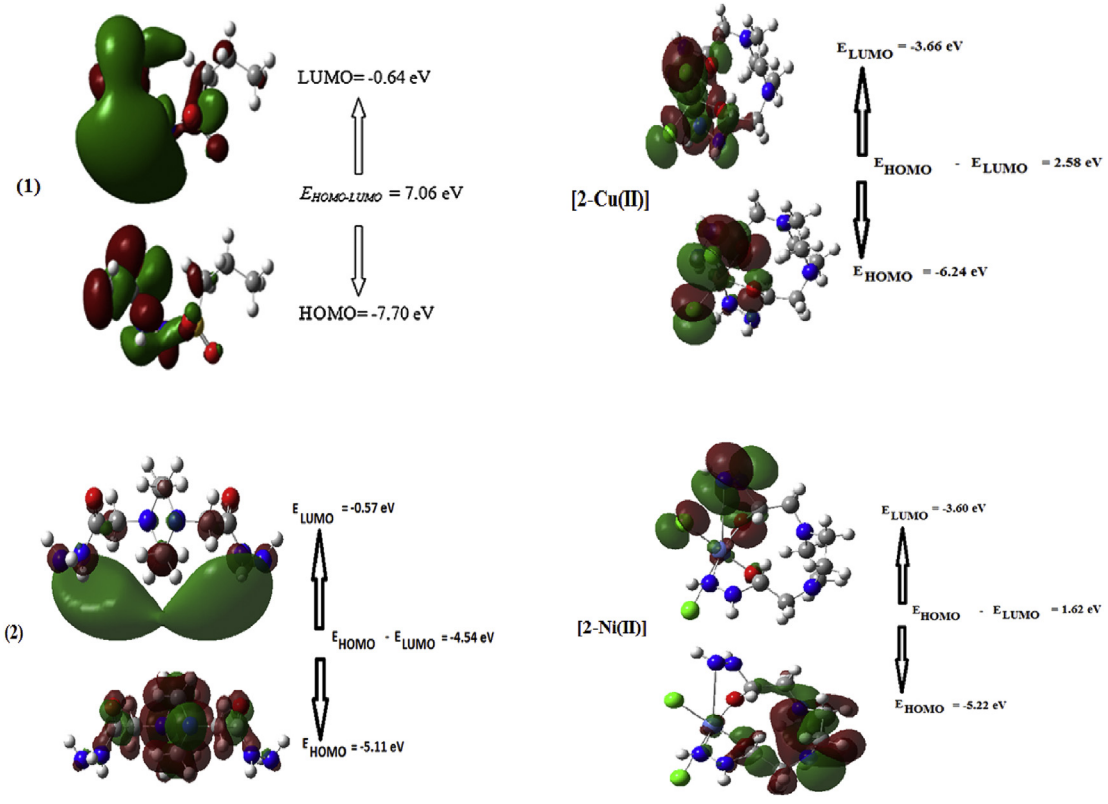

Fig. 6. Plots of the frontier orbitals of compounds.

Table 4
The MICs of antibacterial activity of compounds.

Bacteria strains	MIC μg/mL (mM)				
	(1)	(2)	[2-Ni(II)]	[2-Cu(II)]	SD
Gram- negative					
E coli ATCC 25922	250 (**0,97**)	250 (**1,08**)	62,5 (**0,15**)	31,25 (**0,0725**)	23.4 (**0.088**)
P.aeruginosa ATCC 27853	250 (**0,97**)	125 (**0,54**)	31,25 (**0,074**)	15,125 (**0,036**)	375 (**1.403**)
K.pneumoniae ATCC 70063	250 (**0,97**)	125 (**0,54**)	62,5 (**0,15**)	31,25 (**0,0725**)	23.4 (**0.088**)
Gram-positive					
S. aureus ATCC 25923	250 (**0,97**)	125 (**0,54**)	62,5 (**0,15**)	62,5 (**0,145**)	23.4 (**0.088**)
E.faecalis ATCC 29212	250 (**0,97**)	125 (**0,54**)	62,5 (**0,15**)	31,25 (**0,0725**)	93.75 (**0.35**)
S. typhimurium ATCC 14028	250 (**0,97**)	250 (**1,08**)	62,5 (**0,15**)	31,25 (**0,0725**)	375 (**1.403**)

SD: Sulfisoxazole.

Percentage of inhibition for the compounds exhibited in Fig. 5S that was expressed as excellent activity (120–200%inhibition), good activity (90–100% inhibition), moderate activity (75–85% inhibition), significant activity (50–60%inhibition), negligible activity (20–30% inhibition)and no activity [61,62]. As seen in Fig. 5S, **[2-Cu(II)] and [2-Ni(II)]** show excellent activity while other compounds have good activity or moderate activity against *P.aeruginosa.* **[2-Cu(II)]** exhibit excellent activity against *S. typhimurium*, whereas **[2-Ni(II)]** shows good activity.

4. Conclusion

In the present work, two symmetrical piperazine compounds containing ester, hydrazide moiety nickel (II) and copper (II) have been synthesized and characterized. The room temperature effective magnetic moments of the complexes indicate these compounds are mon-nuclear. The theoretical calculations show that the energy band gap and chemical hardness decreases upon complexation. All compounds show antimicrobial activities against tested bacteria. **[2-Cu(II)] and [2-Ni(II)]** show excellent activity against *P.aeruginosa.* Some relationships between their chemical structure and biological activities are discussed. In the study conducted, it was found that anti-bacterial activity was inversely related to energy band gap (E_{HOMO}-E_{LUMO}) and chemical hardness (η). Also, there is an accurate relationship between antibacterial activity and chemical softness (S) for studied compounds. This will be interesting for their possible application in medical practice in the future. The electrochemical behaviors of piperazine compounds were evaluated by means of cyclic voltammetry (CV), controlled potential electrolysis, and chronoamperometry (CA) techniques. The electrochemical reduction (EC) mechanism supposes that $2e^-$ transferred reduction occurs in two steps. $E_p^c - E_{p/2}^c$ values were found to be 50–130 mV for each peak which is in good agreement with those given in literature for EC systems.

Acknowledgments

The authors would like to thank Ahi Evran University BAP (Grant No: EGT.A3.17.003) for the financial support of this project.

Appendix A. Supplementary data

Supplementary data related to this article can be found at https://doi.org/10.1016/j.molstruc.2018.06.076.

References

[1] G.M. Ziarani, V.F. Vavsari, The role of hydrazide compounds in asymmetric synthesis, Tetrahedron Asymmetry 28 (2017) 203–214.
[2] Ł. Popiołek, Hydrazide–hydrazones as potential antimicrobial agents: overview of the literature, Med. Chem. Res. 26 (2017) 287–301.
[3] S. Mehta, Synthesis and biological activity of pyrrole and pyrrolidine compounds from 4-chloro 2-hydroxybenzoic acid hydrazide, Int. J. Pharm. Res. Bio-Sci. 2 (2013) 382–394. http://www.ijprbs.com/issuedocs/2013/2/IJPRBS311.pdf.
[4] E. Mousavi, S. Tavakolfar, A. Almasirad, Z. Kooshafar, S. Dehghani, A. Afsharinasab, A. Amanzadeh, S. Shafiee, M. Salimi, In vitro and in vivo assessments of two novel hydrazide compounds against breast cancer as well as mammary tumor cells, Canc. Chemother. Pharmacol. 79 (2017) 1195–1203.
[5] I.E. El-Shamy, A.M. Abdel-Mohsen, A.A. Alsheikh, M.M.G. Fouda, S.S. Al-Deyab, M.A. El-Hashash, J. Jancar, Synthesis, biological, anti-inflammatory activities and quantum chemical calculation of some [4-(2, 4, 6-trimethylphenyl)-1(2H)-oxo-phthalazin-2yl] acetic acid hydrazide derivatives, Dyes Pigments 113 (2015) 357–371.
[6] S.R. Patel, R. Gangwal, A.T. Sangamwar, R. Jain, Synthesis, biological evaluation and 3D-QSAR study of hydrazide, semicarbazide and thiosemicarbazide derivatives of 4-(adamantan-1-yl)quinoline as anti-tuberculosis agents, Eur. J. Med. Chem. 85 (2014) 255–267.
[7] A. Sharma, P. Piplani, Design and synthesis of some acridine-piperazine hybrids for the improvement of cognitive dysfunction, Chem. Biol. Drug Des. 90 (2017) 926–935.
[8] R. Zhuang, L. Gao, X. Lv, J. Xi, L. Sheng, Y. Zhao, R. He, X. Hu, Y. Shao, X. Pan, S. Liu, W. Huang, Y. Zhou, J. Li, J. Zhang, Exploration of novel piperazine or piperidine constructed non-covalent peptidyl derivatives as proteasome inhibitors, Eur. J. Inorg. Chem. 126 (2017) 1056–1070.
[9] N. Büyükkıdan, C. Yenikaya, H. Ikimen, C. Karahan, T. Korkmaz, Synthesis, characterization and biological activities of metal(II) dipicolinate complexes derived from pyridine-2,6-dicarboxylic acid and 2-(piperazin-1-yl)ethanol, J. Mol. Struct. 1101 (2015) 139–146.
[10] M.A. Bhata, S.H. Loneb, R.J. Butcherc, S.K. Srivastavaa, Theoretical and experimental investigations into structural, electronic, molecular and biological properties of 4-(3-Chlorophenyl)-1-(3-chloropropyl) piperazin-1-ium chloride, J. Mol. Struct. 1168 (2018) 242–249.
[11] J. Zhang, L. Gao, J. Xi, L. Sheng, Y. Zhao, L. Xu, Y. Shao, S. Liu, R. Zhuang, Y. Zhou, J. Li, Design, synthesis and biological evaluation of novel non-covalent piperidine-containing peptidyl proteasome inhibitors, Bioorg. Med. Chem. 24 (2016) 6206–6214.
[12] C.B. Mishra, R.K. Mongre, S. Kumari, D.K. Jeong, M. Tiwari, Novel triazole-piperazine hybrid molecules induce apoptosis via activation of the mitochondrial pathway and exhibit antitumor efficacy in osteosarcoma xenograft nude mice model, ACS Chem. Biol. 12 (2017) 753–768.
[13] Z.-S. Gu, Y. Xiao, Q.-W. Zhang, J.-Q. Li, Synthesis and antidepressant activity of a series of arylalkanol and aralkyl piperazine derivatives targeting SSRI/5-HT 1A/5-HT 7, Bioorg. Med. Chem. Lett. 27 (2017) 5420–5423.
[14] H. Keypour, M. Mahmoudabadi, A. Shooshtari, M. Bayat, M. Ghassemzadeh, L. Hosseinzadeh, F. Mohsenzadeh, K. Harms, Synthesis and characterization of two new N4O2 macroacyclic Schiff-base ligands containing piperazine moiety and mononuclear Co(III) and Cu(II) complexes, spectral, X-ray crystal structural, theoretical studies, cytotoxic and antibacterial properties, Polyhedron 129 (2017) .189–198.
[15] Y. Zhang, Y.-Z. Zhan, Y. Ma, X.-W. Hua, W. Wei, X. Zhang, H.-B. Song, Z.-M. Li, B.-L. Wang, Chinese Chem, Lett. 29 (2018) 441–446.
[16] S. Zikolova, M. Nikolova, N. Ivanova, Pharmacological Study of the Activity of a Group of Piperizine Esters and Changes in Action Relative to Their Chemical Structure. http://www.ncbi.nlm.nih.gov/pubmed/609596. (Accessed 25 December 2017).
[17] U.A. Mohsen, B. Kocyigit-Kaymakcioglu, E.E. Oruc-Emre, Z.A. Kaplancikli, S. Rollas, Studies on hydrazide-hydrazones derivatives as acetylcholinesterase inhibitors, Marmara Univ. Saglik Bilim. Enst. Derg 5 (2015) 10–14.
[18] C. Fan, J.C. Vederas, Structure-activity relationship (SAR) studies of aryl-hydrazide inhibitors of diaminopimelate aminotransferase, in: Abstr. Pap. 243rd ACS Natl. Meet. Expo. San Diego, CA, United States, March, 25-29, 2012.
[19] D. R. Bolin, C. Michoud, Preparation of (Thio)phenoxyacetamide Derivatives as Inhibitors of Diacylglycerol Acyltransferase, US Patent 0178532, date of patent June 25, 2006.
[20] B. Kaya, L. Yurttaş, B. Nurpelin Sağlik, S. Levent, Y. Özkay, Z.A. Kaplancikli, U. Kaya, L. Yurtta, U. Nurpelin Saglik, Novel 1-(2-pyrimidin-2-yl)piperazine

derivatives as selective monoamine oxidase (MAO)-A inhibitors, J. Enzym. Inhib. Med. Chem. 32 (2017) 193–202.
[21] J. Sun, S.Z. Ren, X.Y. Lu, J.L. Fi, Q.S. Chen, C. Xu, H.L. Zhu, Discovery of a series of 1,3,4-oxadiazole-2(3*H*)-thione derivatives containing piperazine skeleton as potential FAKinhibitors, Bioorg. Med. Chem. 25 (2017) 2593–2600.
[22] M. Le Cam, S. Bernard, S. Cottin, Y. Madec, J.C. Dubin, Mechanisms of in vitro and in vivo action of isonicotinic acid hydrazide and of 2-alkylisonicotinic acid thioamides on some enzymic systems in mouse liver, Ann. Pharm. Fr. 25 (1967) 303–314.
[23] M.D. Arbo, R. Silva, D.J. Barbosa, D. Dias Da Silva, L.G. Rossato, M.D.L. Bastos, H. Carmo, Piperazine designer drugs induce toxicity in cardiomyoblast h9c2 cells through mitochondrial impairment, P Toxicol. Lett. 229 (2014) 178–189.
[24] M. Khatri, S.K. Rai, S. Alam, A. Vij, M. Tiwari, Synthesis and pharmacological evaluation of new arylpiperazines N-{4-[4-(aryl) piperazine-1-yl]-phenyl}-amine derivatives: putative role of 5-HT 1A receptors, Bioorg. Med. Chem. 17 (2009) 1890–1897.
[25] S. Zikolova, L. Zhelyazkov, Synthesis of some piperazine derivatives. I. Preparation of N-mono- and N,N'-disubstituted piperazines with probable antitubercular activity, Farmatsiya 18 (1968) 8–17.
[26] M. Gökçe, S. Utku, E. Küpeli, Synthesis and analgesic and anti-inflammatory activities 6-substituted-3(2H)-pyridazinone-2-acetyl-2-(p-substituted/non-substituted benzal)hydrazone derivatives, Eur. J. Med. Chem. 44 (2009) 3760–3764.
[27] S. Alyar, H. Alyar, U.O. Ozdemir, O. Sahin, K. Kaya, N. Ozbek, A.B. Gunduzalp, Synthesis, characterization, antibacterial activity and quantum chemical studies of N'-Acetyl propane sulfonic acid hydrazide, J. Mol. Struct. 1094 (2015) 237–245.
[28] H. Esener, R. Adiguze, Z. Ergin, E. Aktan, N. Turan, M. Sekerci, Synthesis and characterization of novel Mn(II), Co(III), Ni(II) and Cd(II) complexes from 4-(2-nitrophenylazo)-1H-pyrazole-3,5-diamine, Adv. Sci. Lett. 4 (2011) 1–7.
[29] R. Adıguzel, H. Esener, Z. Ergin, E. Aktan, N. Turan, M. Sekerci, Synthesis and Characterization of Ni(II) and Cd(II) Complexes of 4-(4-Nitrophenylazo)- 1H-pyrazole-3,5-diamine and 4-(4-methylphenylazo)-1H-pyrazole-3,5-diamine. http://www.asianjournalofchemistry.co.in/User/ViewFreeArticle.aspx?ArticleID=23_6_100. (Accessed 29 December 2017).
[30] Ü.Ö. Özdemir, N. Akkaya, N. Özbek, New Nickel (II), Palladium (II), Platinum (II) complexes with aromatic methanesulfonylhydrazone based ligands. Synthesis, spectroscopic characterization and in vitro antibacterial evaluation, Inorg. Chim. Acta. 400 (2013) 13–19.
[31] G.M. Sheldrick, A short history of SHELX, Acta Crystallogr. 64 (2008) 112–122.
[32] G.M. Sheldrick, SHELXS-97, Program for Crystal Structure Solution, University of Göttingen, 1997.
[33] O.V. Dolomanov, L.J. Bourhis, R.J. Gildea, J.A.K. Howard, H. Puschmann, OLEX2: a complete structure solution, refinement and analysis program, J. Appl. Crystallogr. 42 (2009) 339–341.
[34] A.S. Baranski, W.R. Fawcett, C.M. Gilbert, Use of microelectrodes for the rapid determination of the number of electrons involved in an electrode reaction, Anal. Chem. 57 (1985) 166–170.
[35] R.J. Klingler, J.K. Kochi, Electron-transfer kinetics from cyclic voltammetry. Quantitative description of electrochemical reversibility, J. Phys. Chem. 85 (1981) 1731–1741.
[36] L.G. Costa, J.C. Davila, D.A. Lawrence, D.J. Reed (Eds.), John Wiley & Sons, Inc, Hoboken, NJ, USA, 2001.
[37] T. Tunç, Y. Koç, L. Açık, M.S. Karacan, N. Karacan, DNA cleavage, antimicrobial studies and a DFT-based QSAR study of new antimony(III) complexes as glutathione reductase inhibitor, Spectrochim. Acta Part A Mol. Biomol. Spectrosc 136 (2015) 1418–1427.
[38] M.J. Frisch, G.W. Trucks, H.B. Schlegel, G.E. Scuseria, M.A. Robb, J.R. Cheeseman, J.A.Jr Montgomery, T. Vreven, K.N. Kudin, J.C. Burant, J.M. Millam, S.S. Iyengar, J. Tomasi, V. Barone, B. Mennucci, M. Cossi, G. Scalmani, N. Rega, G.A. Petersson, H. Nakatsuji, M. Hada, M. Ehara, K. Toyota, R. Fukuda, J. Hasegawa, M. Ishida, T. Nakajima, Y. Honda, O. Kitao, H. Nakai, M. Klene, X. Li, J.E. Knox, H.P. Hratchian, J.B. Cross, C. Adamo, J. Jaramillo, R. Gomperts, R.E. Stratmann, O. Yazyev, A.J. Austin, R. Cammi, C. Pomelli, J.W. Ochterski, P.Y. Ayala, K. Morokuma, G.A. Voth, P. Salvador, J.J. Dannenberg, V.G. Zakrzewski, S. Dapprich, A.D. Daniels, M.C. Strain, O. Farkas, D.K. Malick, A.D. Rabuck, K. Raghavachari, J.B. Foresman, J.V. Ortiz, Q. Cui, A.G. Baboul, S. Clifford, J. Cioslowski, B.B. Stefanov, G. Liu, A. Liashenko, P. Piskorz, I. Komaromi, R.L. Martin, D.J. Fox, T. Keith, M.A. Al-Laham, C.Y. Peng, A. Nanayakkara, M. Challacombe, P.M.W. Gill, B. Johnson, W. Chen, M.W. Wong, C. Gonzalez, J.A. Pople, Gaussian 03: Revision B.04, Gaussian, Inc, Pittsburgh, PA, 2003.
[39] P.C. Hariharan, J.A. Pople, Accuracy of AH_n equilibrium geometries by single determinant molecular orbital theory, J. Chem. Phys. 27 (1973) 209–214.
[40] A.B. Gündüzalp, N. Özbek, N. Karacan, Synthesis, characterization, and antibacterial activity of the ligands including thiophene/furan ring systems and their Cu(II), Zn(II) complexes, Med. Chem. Res. 21 (2012) 3435–3444.
[41] N. Özbek, S. Alyar, S. Mamaş, E. Şahin, N. Karacan, Synthesis, crystal structure, antibacterial activities, and electrochemical studies of new N, N 0 –polymethylene bis-sulfonamides, J. Mol. Struct. 1010 (2012) 1–7.
[42] N. Özbek, S. Alyar, H. Alyar, E. Sahin, N. Karacan, Synthesis, characterization and anti-microbial evaluation of Cu(II), Ni(II), Pt(II) and Pd(II) sulfonylhydrazone complexes; 2D-QSAR analysis of Ni(II) complexes of sulfonylhydrazone derivatives, Spectrochim. Acta Part A Mol. Biomol. Spectrosc 108 (2013) 123–132.
[43] K. Singh, Y. Kumar, P. Puri, M. Kumar, C. Sharma, Cobalt, nickel, copper and zinc complexes with 1,3-diphenyl-1H-pyrazole-4-carboxaldehyde Schiff bases: antimicrobial, spectroscopic, thermal and fluorescence studies, Eur. J. Med. Chem. 52 (2012) 313–321.
[44] M. Orojloo, P. Zolgharnein, M. Solimannejad, S. Amani, Synthesis and characterization of cobalt (II), nickel (II), copper (II) and zinc (II) complexes derived from two Schiff base ligands: spectroscopic, thermal, magnetic moment, electrochemical and antimicrobial studies, Inorg. Chim. Acta. 467 (2017) 227–237.
[45] W.A. Zoubi, A.A. Salih Al Hamdani, S.D. Ahmed, Y.G. Ko, A new azo-Schiff base: synthesis, characterization, biological activity and theoretical studies of its complexes, Appl. Organomet. Chem. 32 (2018) 1–15.
[46] S.M.E. Khalil, H.S. Seleem, B.A. El-Shetary, M. Shebl, Mono- and Bi-Nuclear metal complexes of schiff-base hydrazone (ONN) derived from o-hydroxyacetophenone and 2-amino-4-hydrazino-6-methyl pyrimidine, J. Coord. Chem. 55 (2002) 883–899.
[47] Ü.Ö. Özdemir, E. Aktan, F. İlbiz, A.B. Gündüzalp, N. Özbek, M. Sarı, Ö. Çelik, S. Saydam, Characterization, antibacterial, anticarbonic anhydrase II isoenzyme, anticancer, electrochemical and computational studies of sulfonic acid hydrazide derivative and its Cu(II) complex, Inorg. Chim. Acta. 423 (2014) 194–203.
[48] M. Saif, M.M. Mashaly, M.F. Eid, R. Fouad, Synthesis and thermal studies of tetraaza macrocylic ligand and its transition metal complexes. DNA binding affinity of copper complex, Spectrochim. Acta Part A Mol. Biomol. Spectrosc. 79 (2011) 1849–1855.
[49] L. Shen, F.W. Wang, A.B. Cheng, S. Yang, 2,2'-(Piperazine-1,4-diium-1,4-diyl) diacetate dihydrate, Acta Crystallogr. 62 (2006) 2242–2244.
[50] S. Sreenivasa, N.R. Mohan, T. Madhu Chakrapani Rao, P.A. Suchetan, P.A. Palakshamurthy, B.S. Vijithkumar, 4-(4-Methyl-phenyl-sulfon-yl)piperazin-1-ium tri-fluoro-acetate, Acta Crystallogr. 69 (2013) 1112–1113.
[51] N.N. Gajera, M.C. Patel, M.M. Jotani, E.R. Tiekink, tert-Butyl 4-{[2-amino-4-(2-hy-droxy-phen-yl)pyrimidin-5-yl]meth-yl}piperazine-1-carboxyl-ate, Acta Crystallogr. 69 (2013) 1577–1578, https://doi.org/10.1107/S1600536813025774.
[52] A. Balaban Gündüzalp, Ü. Özdemir Özmen, B.S. Çevrimli, S. Mamaş, S. Çete, Synthesis, characterization, electrochemical behavior, and antimicrobial activities of aromatic/heteroaromatic sulfonylhydrazone derivatives, Med. Chem. Res. 23 (2014) 3255–3268.
[53] E. Laviron, A multilayer model for the study of space distributed redox modified electrodes: Part I. Description and discussion of the model, J. Electroanal. Chem. 112 (1980) 1–9.
[54] F. Blanco, I. Alkorta, J. Elguero, Spectral assignments and reference data, Magn. Reson. Chem. 45 (2007) 797–800.
[55] A.M.S. Silva, R.M.S. Sousa, M.L. Jimeno, F. Blanco, I. Alkorta, J. Elguero, Experimental measurements and theoretical calculations of the chemical shifts and coupling constants of three azines (benzalazine, acetophenoneazine and cinnamaldazine), Magn. Reson. Chem. 46 (2008) 859–864.
[56] S. Gunasekaran, R.A. Balaji, S. Kumerasan, G. Anand, S. Srinivasan, Experimental and theoretical investigations of spectroscopic properties of N-acetyl-5-methoxytryptamine, J. Can, Anal. Sci. Spectrosc. 53 (2008) 149–160.
[57] T. Koopmans, Über die Zuordnung von Wellenfunktionen und Eigenwerten zu den Einzelnen Elektronen Eines Atoms, Physica 1 (1934) 104–113.
[58] R.G. Pearson, Chemical hardness and density functional theory, J. Chem. Sci. 117 (2005) 369–377.
[59] R.G. Parr, R.G. Pearson, Absolute hardness: companion parameter to absolute electronegativity, J. Am. Chem. Soc. 105 (1983) 7512–7516.
[60] R.K. Roy, K. Choho, F. De Proft, P. Geerlings, Reactivity and stability of aromatic carbonyl compounds using density functional theory-based local and global reactivity descriptors, J. Phys. Org. Chem. 12 (1999) 503–509.
[61] A.B. Gündüzalp, İ. Özsen, H. Alyar, S. Alyar, N. Özbek, Biologically active Schiff bases containing thiophene/furan ring and their copper(II) complexes: synthesis, spectral, nonlinear optical and density functional studies, J. Mol. Struct. 1120 (2016) 259–266.
[62] A.B. Gündüzalp, G. Parlakgümüş, D. Uzun, Ü. Özdemir Özmen, N. Özbek, M. Sarı, T. Tunç, Carbonic anhydrase inhibitors: synthesis, characterization and inhibition activities of furan sulfonylhydrazones against carbonic anhydrase I (hCA I), J. Mol. Struct. 1105 (2016) 332–340.